The Plant Cell, Vol. 25: 202–214, January 2013, www.plantcell.org

Arabidopsis TWISTED DWARF1 Functionally Interacts with Auxin Exporter ABCB1 on the Root Plasma Membrane[CW]

Bangjun Wang,[a,b,c,1] Aurélien Bailly,[a,b,1,2] Marta Zwiewka,[d] Sina Henrichs,[b] Elisa Azzarello,[e] Stefano Mancuso,[e] Masayoshi Maeshima,[f] Jiří Friml,[d,g,h] Alexander Schulz,[c] and Markus Geisler[a,b,3]

[a] Department of Biology-Plant Biology, University of Fribourg, 1700 Fribourg, Switzerland
[b] University of Zurich, Institute of Plant Biology, 8008 Zurich, Switzerland
[c] Department of Plant and Environmental Sciences, University of Copenhagen, 1871 Frederiksberg C, Frederiksberg, Denmark
[d] Department of Plant Systems Biology, VIB and Department of Plant Biotechnology and Bioinformatics, Ghent University, 9052 Gent, Belgium
[e] Department of Horticulture, University of Firenze, 50019 Sesto Fiorentino, Italy
[f] Laboratory of Cell Dynamics, Graduate School of Bioagricultural Sciences, Nagoya University, 464-8601 Nagoya, Japan
[g] Department of Functional Genomics and Proteomics, Central European Institute of Technology (CEITEC), Masaryk University, 62500 Brno, Czech Republic
[h] Institute of Science and Technology Austria (IST Austria), 3400 Klosterneuburg, Austria

Plant architecture is influenced by the polar, cell-to-cell transport of auxin that is primarily provided and regulated by plasma membrane efflux catalysts of the PIN-FORMED and B family of ABC transporter (ABCB) classes. The latter were shown to require the functionality of the FK506 binding protein42 TWISTED DWARF1 (TWD1), although underlying mechanisms are unclear. By genetic manipulation of *TWD1* expression, we show here that TWD1 affects shootward root auxin reflux and, thus, downstream developmental traits, such as epidermal twisting and gravitropism of the root. Using immunological assays, we demonstrate a predominant lateral, mainly outward-facing, plasma membrane location for TWD1 in the root epidermis characterized by the lateral marker ABC transporter G36/PLEIOTROPIC DRUG-RESISTANCE8/PENETRATION3. At these epidermal plasma membrane domains, TWD1 colocalizes with nonpolar ABCB1. In planta bioluminescence resonance energy transfer analysis was used to verify specific ABC transporter B1 (ABCB1)–TWD1 interaction. Our data support a model in which TWD1 promotes lateral ABCB-mediated auxin efflux via protein–protein interaction at the plasma membrane, minimizing reflux from the root apoplast into the cytoplasm.

INTRODUCTION

Intra- and intercellular gradients of the plant hormone auxin are generated by a plant-specific cell-to-cell transport process that is designated as polar auxin transport (PAT; reviewed in Robert and Friml, 2009; Vanneste and Friml, 2009). Due to the chemical properties of the main relevant auxin, indole-3-acetic acid (IAA), PAT is largely under the control of the plasma membrane (PM) efflux complex that is made up of auxin efflux catalysts of the PIN-FORMED (PIN) and the B family of ABC transporter (ABCB)/PGP/MDR classes (Blakeslee et al., 2007; Mravec et al., 2008). ABCBs and PINs contribute to PAT independently for the most part (Blakeslee et al., 2007; Mravec et al., 2008), and this is reflected by generally distinct mutant phenotypes. Full-length PINs, which arose with the first land plants (Galván-Ampudia and Offringa, 2007), have mainly polar expression patterns and provide the basis for vectorial mass transport of auxin (Geisler and Murphy, 2006). On the other hand, ancient ABCBs are mainly multilaterally expressed and are thought to function primarily in minimizing apoplastic reflux in apical tissues with high auxin content (Geisler et al., 2005; Geisler and Murphy, 2006; Matsuda et al., 2011).

Whereas regulation of PIN-mediated auxin efflux is well characterized on both the transcriptional and posttranscriptional levels, significantly less is known for ABCBs. Current work has focused on the interaction of ABC transporter B1/P-GLYCOPROTEIN1 (ABCB1/PGP1) and ABC transporter B19/P-GLYCOPROTEIN19/MULTIDRUG-RESISTANCE1 (ABCB19/PGP19/MDR1) with the FK506 binding protein42 TWISTED DWARF1 (TWD1; Bailly et al., 2008). Physiological and growth defects in *twd1* are caused by strongly reduced auxin efflux capacities in *twd1* and *abcb1 abcb19* leading to similarly reduced long-range IAA transport, which results in elevated or reduced auxin accumulation in *abcb1 abcb19* and *twd1* roots and shoots, respectively (Bailly et al., 2008). This is documented by a close overlap between *twd1* and *abcb1 abcb19* dwarf phenotypes and undirected helical disorientation of overall plant growth. However, *abcb1 abcb19* mutants

[1] These authors contributed equally to this work.
[2] Current address: University of Zurich, Institute for Plant Biology, Department of Microbiology, 8008 Zurich, Switzerland.
[3] Address correspondence to markus.geisler@unifr.ch.
The author responsible for distribution of materials integral to the findings presented in this article in accordance with the policy described in the Instructions for Authors (www.plantcell.org) is: Markus Geisler (markus.geisler@unifr.ch).
[C] Some figures in this article are displayed in color online but in black and white in the print edition.
[W] Online version contains Web-only data.
www.plantcell.org/cgi/doi/10.1105/tpc.112.105999

show less severe dwarfism, suggesting malfunction of additional components (Geisler and Bailly, 2007). This holds true also for the stronger disorientation of epidermal layers (twisting) in *twd1* roots and hypocotyls (Geisler et al., 2003; Geisler and Bailly, 2007; Bailly et al., 2008). This is, in contrast with alleles carrying mutations in microtubules or microtubule-associated proteins, not fixed-handed (Hashimoto, 2002; Weizbauer et al., 2011), making a direct connection to microtubule dynamics unlikely.

Epidermal twisting in *twd1* was recently shown to be partially rescued by application of the diagnostic auxin transport inhibitor 1-*N*-naphtyl-phthalamic acid (NPA). This suggests that at least a part of this phenotype is the result of defects in PAT (Wu et al., 2010). Interestingly, both ABCBs and TWD1 have been shown to bind NPA resulting in disruption of ABCB–TWD1 interaction and, thus, ABCB inhibition (Bailly et al., 2008). As a consequence, *abcb1 abcb19* and *twd1* root gravitropism, although reduced, is less sensitive to NPA (Bailly et al., 2008).

All of these data are consistent with the suggestion that TWD1 acts as a positive modulator of ABCB-mediated auxin efflux by means of physical interaction (Bouchard et al., 2006; Bailly et al., 2008). Currently, however, it is unclear if (and how) TWD1 regulates ABCB-mediated auxin transport directly by ABCB activation or indirectly. Recently, for the first time, a mechanistic insight into the mode of plant ABCB regulation by TWD1 has been provided: TWD1 was shown to interact with the AGC kinase, PINOID (PID), and to direct PID-mediated phosphorylation of ABCB1 in a regulatory linker domain that alters ABCB1 activity (Henrichs et al., 2012). Interestingly, the overall mechanism of ABCB1 regulation by PID resembles that of ABCB19 regulation by phot1 (Christie et al., 2011). Alternatively, TWD1 has been suggested to be responsible for PM targeting from the endoplasmic reticulum (ER) (Wu et al., 2010). However, TWD1–ABCB interaction and its direct impact on auxin fluxes have not yet been addressed in planta.

Here, by analyzing physiological parameters and auxin fluxes in newly described *TWD1* gain-of-function alleles, we demonstrate an essential role for TWD1 in regulation of root architecture and physiology. We show that TWD1 colocalizes and interacts with ABCB1 on specific lateral PM domains of epidermal cell files, suggesting a regulatory role for TWD1 in the reversal of apoplastic reflux and the separation of basal and apical auxin streams in the root.

RESULTS

TWD1 Influences Auxin-Mediated Root Architecture, Including Epidermal Root Twisting

Previous work revealed that *twd1* plants have longer primary roots in the dark, an effect that is reverted when grown under light conditions (Geisler et al., 2003; Figure 1A). This behavior in the dark was reversed by overexpressing a hemagglutinin (HA)-tagged version of TWD1 in the *twd1-3* background that lacks its C-terminal in-plane membrane anchor (HA-TWD1-C_t). Interestingly, under long days this was reverted, and *twd1-3* and HA-TWD1-C_t were indistinguishable under short-day light conditions (Figure 1A), while overexpression of the full-length version of TWD1 (HA-TWD1) resulted in wild-type performance.

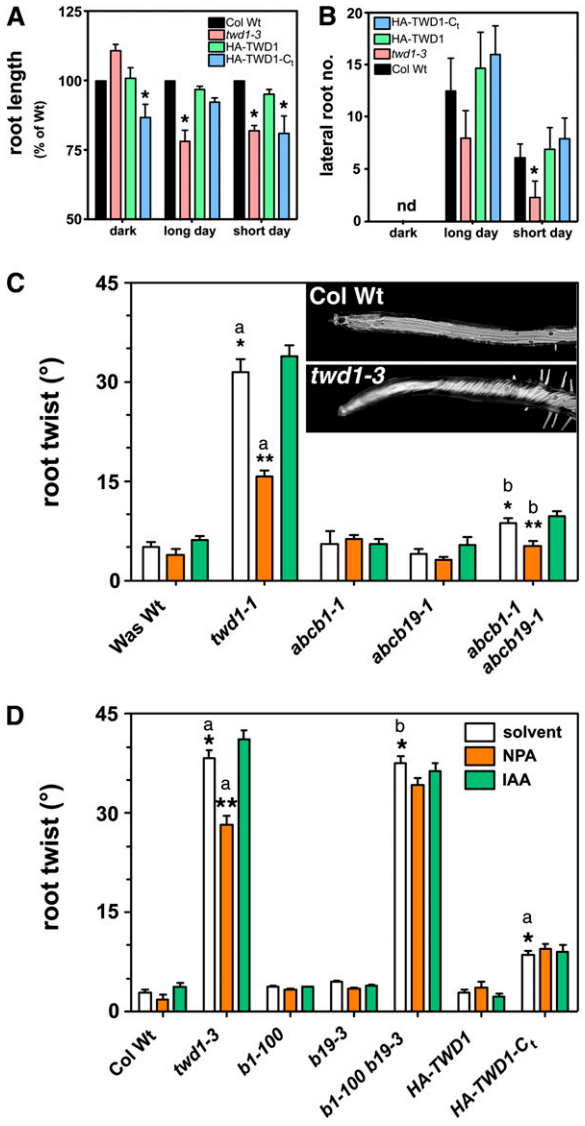

Figure 1. Epidermal Twisting in *abcb1 abcb19* Roots Is Ecotype Dependent.

(A) and **(B)** Primary root length **(A)** and LR number **(B)** of wild-type (Col Wt), *twd1-3*, HA-TWD1, and HA-TWD1-C_t lines grown under indicated light conditions and measured at growth stages 1 and R6 (Boyes et al., 2001), respectively. Mean ± SD; $n \geq 30$. Significant differences (unpaired *t* test with Welch's correction: $P < 0.01$) to wild-type are indicated by an asterisk. nd, not determined.

(C) and **(D)** Quantification of epidermal orientation (angles to the growth direction) using agarose imprints of *TWD1*- and *ABCB1/ABCB19* loss- and gain-of-function roots generated from Ws (Ws Wt; **[C]**) or Col (Col Wt; **[D]**) grown on solvent control, 1 μM NPA, or 100 nM IAA under 8-h light conditions. Mean ± SD; $n \geq 25$. Significant differences (unpaired *t* test with Welch's correction: a, $P < 0.01$; b, $P < 0.05$) to wild-type or solvent control are indicated by one or two asterisks, respectively.

[See online article for color version of this figure.]

The opposite was found for secondary or lateral root (LR) development, another parameter for auxin-controlled plant development. While *twd1-3* displayed fewer LRs at growth stage R6 (Boyes et al., 2001), both overexpression lines HA-TWD1 and HA-TWD1-C_t showed a comparable number of LRs (Figure 1B).

A further hallmark of the Twisted Dwarf1 syndrome is a drastic helical disorientation of epidermal layers (Geisler et al., 2003), which was previously reported as missing in loss-of-function alleles of interacting auxin exporters, ABCB1 (B1) and ABCB19 (*abcb1-a abcb19-1*) generated in the Wassilewskija (Ws) background (Geisler et al., 2003; Bouchard et al., 2006; Bailly et al., 2008). In disagreement, a recent study reported epidermal root twisting for the Columbia (Col) *abcb1-100 abcb19-3* allele, without offering, however, any quantification (Wu et al., 2010). In order to solve this discrepancy, we thoroughly quantified epidermal twisting of a series of *TWD1* loss- and gain-of-function alleles, which is best visualized in the root distal elongation zone (Figure 1C, inset). As reported before, root twisting in both investigated *twd1* alleles, *twd1-1* (Ws background: 31.4°) and *twd1-3* (Col background: 38.4°), was significantly enhanced compared with the corresponding wild-type ecotypes (Ws wild type, 5.1°; Col wild type, 2.9°; Figures 1C and 1D). Root twisting was not fixed-handed and even changed its orientation in closely related root parts. However, the orientation showed a certain preference to be left-handed (81.6% in *twd1-3*; 77.9% in *abcb1-100 abcb19-3*). Root twisting was not significantly different from Ws wild type in *b1-1* (5.6°) and *b19-1* (4.0°) single loss-of-function alleles but was slightly and significantly enhanced in *b1-1 b19-1* (8.6° ± 5.6°; Figure 1C). In comparison to the Ws *b1-1 b19-1* allele, helical disorientation was, like for *twd1-3* (38.4°), drastically enhanced in the Col allele *b1-100 b19-3* (37.5°; Wu et al., 2010), indicating ecotype-specific differences. These observations are also reflected by the finding that twisting in Ws wild type was roughly twofold enhanced compared with Col wild type. Interestingly, overexpression of a HA-tagged version of TWD1 lacking the C-terminal membrane anchor (HA-TWD1-Ct) but not overexpression of the entire TWD1 (HA-TWD1) enhanced epidermal twisting slightly but significantly (8.5° ± 4.1°; Figure 1D).

In agreement with the previous study by Wu et al. (2010), we also found significant rescue of twisting in both *twd1* alleles by NPA. The fact that rescue by NPA was significantly reduced in *b1-100 b19-3* compared with *twd1-3* is in line with the idea that ABCBs are the primary NPA targets (Kim et al., 2010). Interestingly, in both TWD1 overexpression (TWD1-OX) lines, NPA also enhanced root twisting slightly. This is in line with the concept that TWD1 functions as target of NPA functionality (Murphy et al., 2002; Geisler et al., 2003; Bailly et al., 2008). A further notable finding was that IAA slightly increased root twisting in the wild type and most alleles tested, although in a function that is probably independent from TWD1 because it was also found in *twd1*.

In summary, these findings support the role of TWD1 as a regulator of root architecture and the concept that at least a portion of the cellular twist in *twd1* is directly caused by PAT defects (Wu et al., 2010). PAT defects are most probably caused by loss of B1/B19 capacity that is at least to a certain degree ecotype specific.

TWD1 Regulates Root Bending and Shootward Auxin Fluxes

This concept was tested by quantifying root gravitropism kinetics of both TWD1-OX lines, thereby offering an established test system for auxin-regulated root physiology. At early bending (up to 90 min after initiation of gravitropism), *twd1-3*, like HA-TWD1-C_t, showed reduced root bending and bending kinetics (rate of curvature) compared with the wild type (Figures 2A and 2B), while HA-TWD1 was hyperbending at early stages as was shown previously (Bailly et al., 2008). At mid-bending (2 to 3 h), HA-TWD1-C_t showed the highest bending rates resulting in higher final (4 h) curvature for both TWD1-OX alleles (Figure 2B, inset).

Changed root gravitropism rates described for *TWD1* gain-of-function lines argue for altered auxin transport capacities as underlying molecular mechanisms. Using radiolabeled IAA tracers, a reduction in PAT from the root tip to the shoot in *twd1* was recently reported (Geisler et al., 2003; Wu et al., 2010). PAT was widely unchanged in HA-TWD1 but drastically inhibited in HA-TWD1-C_t roots. These reductions are obviously in agreement with reduced root lengths found for HA-TWD1-C_t (Figure 1A).

In order to back up these rather invasive PAT experiments and to enhance resolution, we assayed and imaged basipetal (shootward) transport of *TWD1* gain- and loss-of-function lines in the root on the tissue/organ level using two noninvasive measurements: the auxin-responsive element DR5:GFP (for green fluorescent protein; Ottenschläger et al., 2003) and an auxin-selective, external microelectrode (Mancuso et al., 2005).

Computer-assisted quantification of DR5:GFP signals (for details, see Supplemental Figure 1 online) in HA-TWD1 root tips revealed a slightly reduced but overall similar total DR5:GFP expression in the columella and stele compared with the wild type in the absence and presence of a 2-h gravistimulus (Figures 2C and 2D). However, both *twd1-3* (Bailly et al., 2008) and HA-TWD1-C_t roots showed significantly less total columella and stele signals (Figures 2C to 2E). Reduction in the columella cells is probably not caused by morphological changes in the root tip, judging by staining of starch-containing statocysts (see Supplemental Figure 2 online): *twd1* and *abcb1 abcb19* alleles showed a slightly compressed root tip architecture, although the overall organization of columella cells was widely intact and showed no obvious developmental defects in both of the TWD1-OX lines. This was further supported by experiments where DR5:GFP expression was upregulated by IAA application to the lower sides of roots: Nanomolar concentrations of IAA heavily induced DR5 signals at the side of application except in *twd1* where stimulation was limited to epidermal and endodermal cell files (see Supplemental Figure 1 online).

Quantification of epidermal DR5:GFP reflux signals (Figure 2F; see Supplemental Figure 1 online) confirmed slightly reduced basipetal reflux for *twd1* (Bailly et al., 2008) but indicated enhanced IAA accumulation for HA-TWD1 and HA-TWD1-C_t roots in the absence of a gravistimulus. As expected, gravistimulation improved the epidermal DR5:GFP signal in both of the TWD1-OX lines, but not in *twd1*, giving a rationale for the severe root growth defects in *twd1* (Bailly et al., 2008; Wu et al., 2010). However, the magnitude of gravistimulated, shootward IAA reflux in HA-TWD1 and HA-TWD1-C_t was even slightly below the

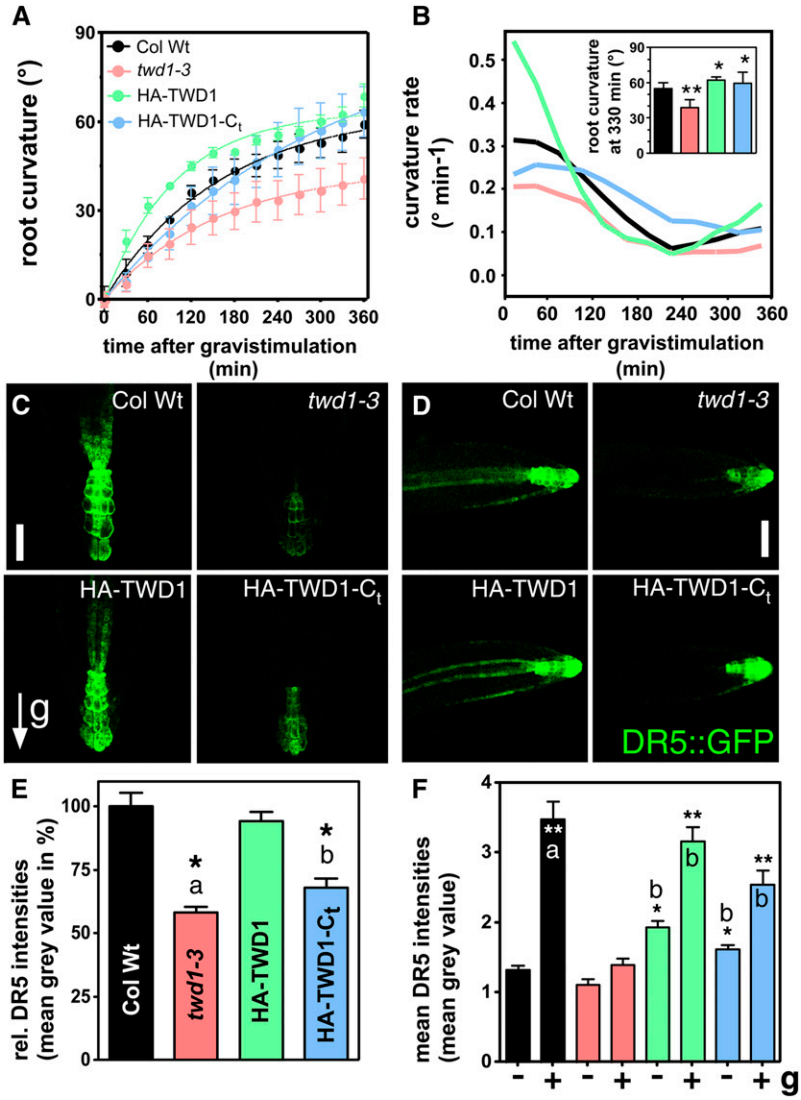

Figure 2. *TWD1* Loss and Gain of Function Alter Root Bending and Shootward Auxin Accumulation

(A) and **(B)** Curvature **(A)** and curvature rates (**[B]**; first deviation of curvature) of *TWD1* loss- (*twd1-3*) and gain-of-function lines with (HA-TWD1) and without the C-terminal membrane anchor (HA-TWD1-C_t). Mean ± SE; n = 8. Inset, curvature at 330 min; significant differences (unpaired t test with Welch's correction) to wild-type (Wt) control are indicated by one ($P < 0.01$) or two asterisks ($P < 0.05$), respectively.

(C) to **(F)** Confocal images (**[C]** and **[D]**) and quantification (**[E]** and **[F]**) of columella (**[C]** and **[E]**) or lower side epidermal signals (**[D]** and **[F]**) of the auxin-responsive reporter DR5:GFP (green) in wild-type (Col Wt), *twd1-3*, HA-TWD1, and HA-TWD1-C_t roots with (+g) and without (−g) gravistimulation. For details of quantification, see Supplemental Figure 1 online. Note reduced expression of DR5:GFP in the columella of *twd1-3* and HA-TWD1-C_t roots and enhanced basipetal accumulation in the lower side epidermis of HA-TWD1 and HA-TWD1-C_t roots. Bars = 50 μm in **(C)** and 100 μm in **(D)**; means ± SE; n = 12. Orientation to the gravity vector (g) is indicated by an arrow.

[See online article for color version of this figure.]

maximum (equal to the wild type) level, suggesting that it was the higher/lower steady state IAA level in nongravistimulated HA-TWD1/HA-TWD1-C_t and *twd1* roots that probably accounted for higher and lower bending kinetic capacities in TWD1-HA/ HA-TWD1-C_t and *twd1*, respectively (Figure 2F).

Using an auxin-selective electrode allows indirect quantification of IAA influx into root surface cell layers, which is an indirect measure for root cap and epidermal auxin concentrations and, therefore, also for auxin movements in these tissues. In the wild type, IAA influx peaks typically at roughly 200 μm from the root tip (see Supplemental Figure 3 online; Santelia et al., 2005; Bailly et al., 2008; Kim et al., 2010; Henrichs et al., 2012).

To better illustrate the spatial arrangement of IAA concentrations in the root tip, we projected measured influx data to a standard root tip model (Swarup et al., 2005) by normalizing the values against confocal root pictures of wild-type and

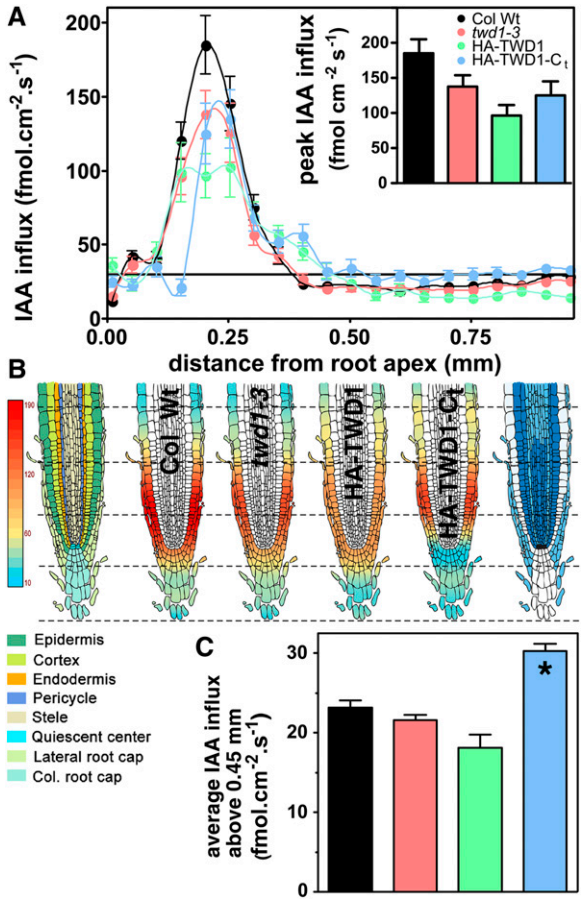

Figure 3. IAA Influx Profiles along TWD1 Loss- and Gain-of-Function Roots Measured Using an IAA-Specific Microelectrode.

(A) and **(B)** Influx profiles **(A)** and heat map presentation **(B)** of IAA influx along wild-type (Col Wt), *twd1-3*, HA-TWD1, and HA-TWD1-C_t roots. Positive fluxes represent a net IAA influx. Data are means ± SE (n = 12). As reference, mapping of root tissues (left) and of high-resolution IAA contents (right; Petersson et al., 2009) is given. For construction of heat maps, see Supplemental Figure 3 online; dashed lines indicate 100-μm distances from the root tip.

(C) Quantification of IAA influx profiles above 0.45 mm from the root tip.

mutant alleles (for details, see Supplemental Figure 3 online). These root maps better illustrate published root surface transport defects in *abcb* (see Supplemental Figure 4 online) and *twd1* roots (Figure 3; see Supplemental Figure 4 online; Bailly et al., 2008) and are complementary to recent IAA mapping using cell sorting that gives only low resolution for the epidermal layer (Petersson et al., 2009).

Root maps (Figure 3B) and the original graph presentation (Figure 3A) clearly indicate reduced influx maxima for *twd1-3* and HA-TWD1-C_t at 200 μm from the root tip (Figure 3A, inset), indicating elevated IAA levels in these domains of the LR cap. In agreement with PAT data, influx peaks for *twd1-3* and HA-TWD1-C_t resemble each other in shape and amplitude, while influx into TWD1-HA roots, showing the most prominent changes in gravitropism, displays a reduced maximum peak but a more compact and broader distribution with two maxima (see Discussion). Interestingly, the average IAA influx into HA-TWD1-C_t roots was significantly enhanced in root regions above 450 μm from the root tip, pointing to altered PAT in a shootward direction.

In summary, these results employing DR5:GFP imaging and IAA-selective microelectrode and radiolabeled IAA tracers provide evidence for defects in basipetal PAT leading to altered root auxin accumulation in *twd1-3* and HA-TWD1-C_t roots. Reduced basipetal transport capacities for *twd1* and HA-TWD1-C_t roots were obviously in line with enhanced accumulation of free IAA reported in these roots and might therefore account for defects in their epidermal cell orientation.

TWD1 Shows Polar PM Signals in the Epidermis Colocalizing with ABCB1

Using a wide range of methods and constructs, TWD1 has been localized independently to several membrane locations, including the PM (Geisler et al., 2003), the tonoplast (Kamphausen et al., 2002), and the ER (Wu et al., 2010). While PM and tonoplast locations were identified using HA-TWD1 by means of immunolocalization followed by either confocal analysis or electron microscopy, ER locations were detected using a C-terminal cyan fluorescent protein (CFP) fused to a genomic stretch of TWD1 (Wu et al., 2010).

To further substantiate these localization data, we employed whole-mount immunolocalizations using four independent antisera raised against two different epitopes of the N-terminal PPIase/FKBP domain of TWD1 (see Methods). In agreement with results obtained using HA-TWD1 (Kamphausen et al., 2002; Geisler et al., 2003), all four antisera consistently labeled PM locations in wild-type roots, mainly limited to epidermal layers (Figure 4) and some layers in the stele (Figures 4L to 4N). Remarkably, in the root epidermis, TWD1 immunodecoration was most pronounced at lateral PM domains, where the outward-facing side showed stronger labeling (Figures 4A to 4D). Lateral outward-facing TWD1 locations perfectly matched those of the lateral PM marker PEN3/ABCG36-GFP (Langowski et al., 2010), a recently described exporter of auxinic compounds, including the native auxin, indole-3-butyric acid (IBA) (Ruzicka et al., 2010). By contrast, colocalization with the nonpolar PM marker BRI1-GFP was limited to lateral subdomains (Figures 4E to 4H). However, while PEN3 showed only an outward-facing lateral signal, the TWD1 lateral signal was found on both sides. Moreover, TWD1 was occasionally found at the basal (rootward) ends of distinct cell files in the stele (Figures 4L to 4N).

Both lateral and basal signals were found with the two ecotypes Col wild type and Landsberg *erecta* wild type and are specific, as the loss-of-function allele *twd1-3* (Geisler et al., 2003) showed only a very faint background, cytoplasmic signal (see Supplemental Figure 5 online). A stronger outward-facing labeling due to incomplete antisera penetration could be excluded using TWD1/PIN1 double labeling (see Supplemental Figure 5 online). Furthermore, TWD1 location and expression seemed to be widely independent of other auxin efflux complex components, like ABCB1, ABCB19, and PIN2 (see Supplemental Figure 5 online).

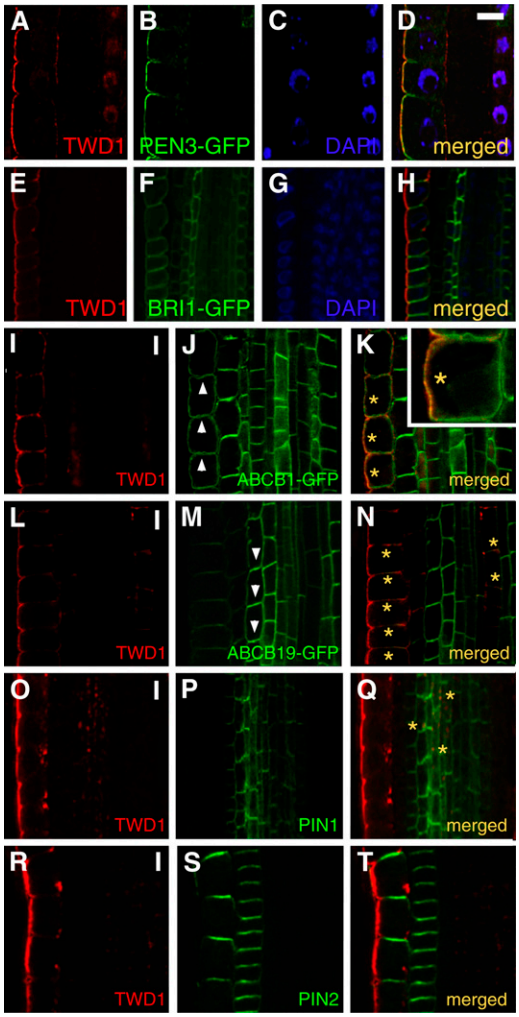

Figure 4. TWD1 Reveals a Lateral PM Location in the Root Epidermis Where It Colocalizes with PEN3/ABCG36 and ABCB1.

(A) to **(H)** Whole-mount immunostaining using anti-TWD1 with PM markers PEN3/ABCG36-GFP (**[A]** to **[D]**) and BRI1-GFP (**[E]** to **[H]**). Note predominant lateral PM localization (**[A]**; stronger at the outer polar domain) in the root epidermis, which matches outward-facing, lateral domains of polar marker PEN3/ABCG36-GFP **(D)** but only partially overlaps the nonpolar marker BRI1-GFP **(H)**. Note that a weak nuclear TWD1 signal in **(A)** is probably caused by bleed-through of the DAPI signal because it was not found without DAPI. Bar = 15 μm.

(I) to **(T)** TWD1 colocalizes with ABCB1-GFP (**[I]** to **[K]**) and occasionally also with ABCB19-GFP (**[L]** to **[N]**) on lateral and basal domains in the epidermis and stele, respectively. Note only partial overlap with PIN1-GFP (**[O]** to **[Q]**) and absence of overlap with PIN2-GFP (**[R]** to **[T]**). Arrowheads indicate directions of main shootward **(J)** and rootward **(M)** auxin flows in the epidermis and endodermis, correlating with main B1 **(J)** and B19 **(M)** expression, respectively. Note that B1-TWD1 and B19-TWD1 colocalization is limited to subdomains in the epidermis (**[K]** and **[N]**) and stele **(N)**, respectively (marked by asterisks). Bars = 10 μm.

Polar PM locations of TWD1 prompted us to analyze B1- and B19/TWD1 colocalizations in detail. Employing TWD1 immunolocalization, we found epidermal colocalization with ABCB1-GFP that was mainly restricted to outward-facing lateral sides with a concentration on lateral corners at cell junctions (Figures 4I to 4K and 4K inset). TWD1/B19-GFP colocalization was only occasional and limited to basal ends of cell files in the stele and to the epidermis, where B19 was weakly but significantly expressed as well (see asterisks in Figure 4N). Overlapping expression in these tissues is obviously in line with suggested involvements of ABCB1 and B19 in basipetal and acropetal PAT streams in the root (Geisler et al., 2003; Bouchard et al., 2006; Wu et al., 2010).

Finally, we analyzed overlap of TWD1 with PIN2 and PIN1, known to provide vectorial streams for PAT routes overlapping with ABCB1 and B19 (Wisniewska et al., 2006), respectively. However, in contrast with ABCB1 and B19, TWD1 and PIN1/PIN2 locations in the root were widely distinct, and overlaps were found only occasionally for PIN1-TWD1 in the stele (Figures 4O to 4T).

TWD1, ABCB1, and B19 Probably Use the Same BFA-Sensitive Trafficking Pathway

This drastic discrepancy in TWD1 localizations using two independent, but by themselves convincing, approaches (either on the ER by fluorescent protein fusion [Wu et al., 2010] or on the PM by immunocytochemistry [this study]) prompted us to reanalyze reported ER locations for TWD1-CFP (Wu et al., 2010) in the shoot. Using identical marker lines as in Wu et al. (2010), we found, to our surprise, in the epidermis of first true leaves CFP signals that widely overlapped with the PM markers 29-1-GFP and FM4-64 (see Supplemental Figure 6 online). However, while both PM markers were uniformly distributed on the PM, TWD1 was spread more unevenly, forming brighter and weaker regions. To verify these microscopy data, we performed immunoblot analyses of TWD1-CFP *Arabidopsis thaliana* microsomes prepared from plants grown in liquid cultures in the presence and absence of light (root-enriched material) followed by separation using linear Suc gradient centrifugation (Geisler et al., 2003). Immunopositive fractions independent of light conditions perfectly aligned with both of the PM markers, H^+-ATPase AHA2, and the aquaporin, PIP (see Supplemental Figure 7 online). These data verify published PM locations using 35S:HA-TWD1 (Geisler et al., 2003), 35S:TWD1-GFP, and 35S:TWD1-YFP (for yellow fluorescent protein) when expressed in leaf mesophyll protoplasts using leaf infiltration (Henrichs et al., 2012).

Colocalization between TWD1 and ABCB proteins led us to investigate whether TWD1 uses the same trafficking pathways as its interacting ABCBs. Brefeldin A (BFA), a drug that interferes with the GNOM-dependent trafficking of PM proteins by concentrating them in large cytoplasmic aggregates, referred to as BFA compartments, has been shown to block ABCB1 but not ABCB19 trafficking (Titapiwatanakun et al., 2009).

Treatments with 20 μM BFA for 1 h efficiently blocked TWD1 trafficking, resulting in colocalization with PM 29-1-GFP but not the ER marker ER-YFP in BFA compartments of the root epidermis (Figures 5A to 5F). BFA also induced colocalization of TWD1 with ABCB1-GFP in epidermal BFA compartments (Figures 5G to 5J). In contradiction to a previous report (Titapiwatanakun et al., 2009)

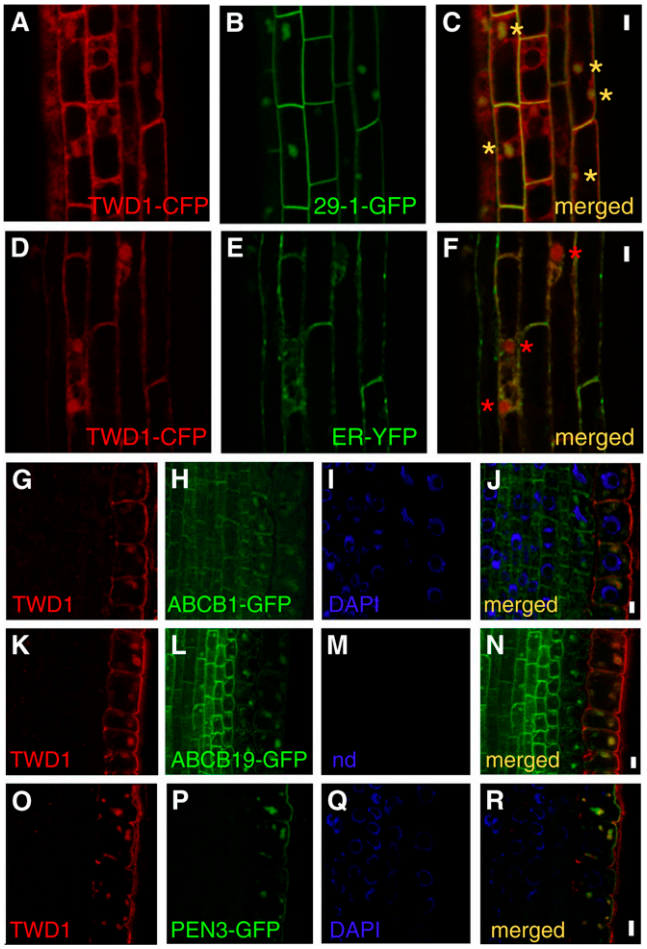

Figure 5. TWD1 Colocalizes with PM Proteins, Including ABCB1, in BFA Compartments

(A) to **(F)** TWD1-CFP (red) colocalizes with PM marker 29-1-GFP (**[A]** to **[C]**, green) but not with ER marker ER-YFP (**[D]** to **[F]**, green) in BFA-induced compartments (20 μM, 1 h). Bars = 10 μm.
(G) to **(R)** Immunodecoration of TWD1 (red) in ABCB1-GFP (**[G]** to **[J]**, green), ABCB19-GFP (**[K]** to **[N]**, green), and PEN3-GFP (**[O]** to **[R]**, green) lines indicate colocalization in BFA-induced compartments (50 μM, 45 min). DAPI stains are in blue. Bars = 5 μm.

ABCB19 was also found to colocalize with TWD1 in BFA compartments, shown by TWD1 immunolocalization using B19-GFP lines (Figures 5K to 5N). Moreover, we found colocalization in BFA compartments between TWD1 and PEN3-GFP (Langowski et al., 2010). In summary, this indicates that TWD1, B1, B19, and PEN3 probably use the same BFA-sensitive trafficking pathway. Furthermore, the BFA sensitivity of TWD1 underscores the identification of TWD1 as a PM protein.

TWD1 Physically Interacts with ABCB1 in Planta

Local but clear colocation between ABCB1 and TWD1 at the PM led us to test ABCB1/TWD1 interactions in planta using bioluminescence resonance energy transfer (BRET). BRET offers substantial advantages over alternative techniques, such as fluorescence resonance energy transfer and bimolecular fluorescence complementation as its quantification is reliable and its interaction reversible. Previously, BRET was successfully employed for demonstrating ABCB1/TWD1 interaction in yeast (Bailly et al., 2008) and TWD1-PID in tobacco (*Nicotiana benthamiana*) (Henrichs et al., 2012). In order to do so, N- and C-terminal YFP- and *Renilla* luciferase (Rluc)–tagged combinations of TWD1 and ABCB1 (Henrichs et al., 2012) were stably coexpressed under the control of the constitutive cauliflower mosaic virus 35S promoter in their corresponding mutant *Arabidopsis* backgrounds or transfected in *N. benthamiana* leaves by *Agrobacterium tumefaciens* infiltration. In analogy to Rluc versions of TWD1 (Henrichs et al., 2012), YFP fusions of TWD1 complemented *twd1* phenotypes (Figure 6; see Supplemental Figure 8 online).

Interestingly, although expressed under a strong, constitutive promoter, TWD1-YFP and YFP-TWD1 expression was mainly limited to the LR cap and epidermal and cortical root layers, while there was additional labeling in the stele (Figure 6; see Supplemental Figure 8 online). *Agrobacterium*-mediated leaf infiltration of tobacco leaves using the same construct resulted in a clear PM labeling (Henrichs et al., 2012). However, TWD1-YFP and YFP-TWD1 displayed a mix of PM and ER signals in the root meristematic zone, the leaf epidermis, and guard cells (Figure 6; see Supplemental Figure 8 online). Therefore, we reanalyzed TWD1-YFP by employing PM and ER markers, FM4-64 and hexyl rhodamine B, respectively. Wide colocalization between TWD1-YFP and hexyl rhodamine B clearly indicated ER locations for TWD1 (Figure 6F). However, we also found TWD1-YFP signals surrounding the cells that did not overlap with hexyl rhodamine B (green signals in merged picture in Figure 6F). These were identified as PM signals by TWD1-YFP/FM4-64 colocalization (yellow signals in merged picture in Figure 6E; see Supplemental Figure 9 online). Moreover, we verified these pharmacological data by coimaging 35S:TWD1-YFP with PM marker ABCB19:ABCB19-CFP. Indeed, PM colocations were found but mainly limited to certain planar, epidermal cell files (see Supplemental Figures 10A to 10C online). Quantification of colocalization resulted in correlation coefficients of roughly 0.6 for epidermal PMs, indicating a significant colocalization that was not found for the inner part of the cells (see Supplemental Figure 10D online). Colocalization of TWD1-YFP and B19-CFP on BFA bodies further supported that a portion of TWD1-YFP was found on the PM (see Supplemental Figures 10E to 10G online).

Finally, to verify the microscopy data, we performed immunoblot analyses of YFP-TWD1 and TWD1-YFP of *Arabidopsis* microsomes separated by linear Suc gradient centrifugation (Geisler et al., 2003). Both TWD1 fusions perfectly aligned with the PM markers H^+-ATPase (AHA2), aquaporin (PIP), and TWD1-CFP (see above and Supplemental Figure 7 online). The lack of a clear ER signal in the immunoblot analyses of 35S:TWD1-YFP/YFP-TWD1 and TWD1:TWD1-CFP might have been caused by use of different growth conditions (here, whole seedlings grown under mixotrophic conditions). However, in summary, this subset of data supports that at least a portion of TWD1-YFP resides on the PM and justifies the usage of TWD1-YFP in subsequent BRET experiments.

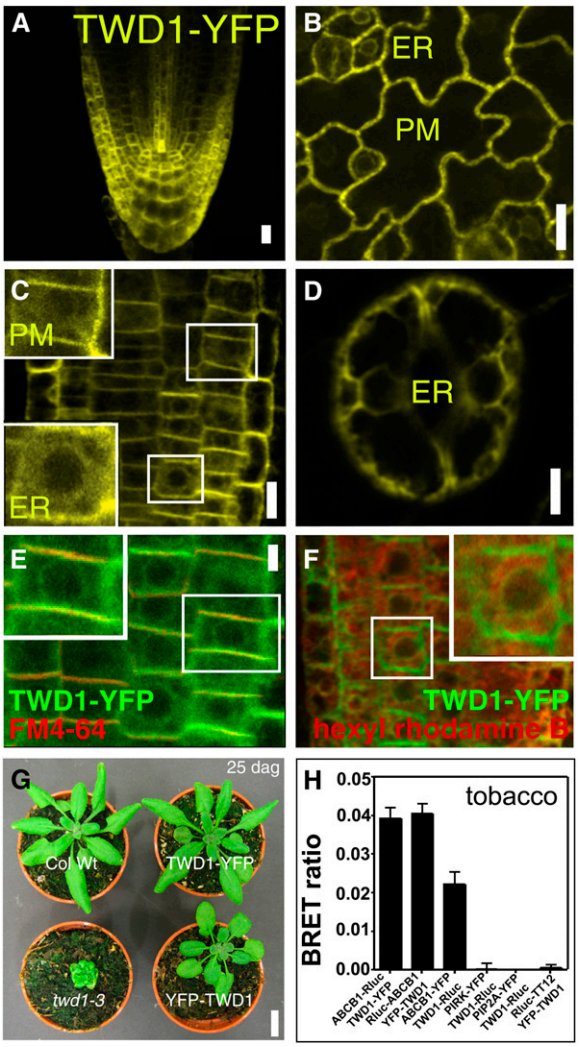

Figure 6. TWD1 Interacts with ABCB1 in Planta.

(A) to **(D)** Expression of TWD1-YFP in the *Arabidopsis* root tip **(A)**, leaf epidermis **(B)**, root meristematic zone epidermis **(C)**, and guard cells **(D)** indicating a dual location at the PM and the ER. Insets, magnification of PM and ER signals in the root meristematic zone. Bars = 20 μm in **(A)**, 10 μm in **(B)**, 15 μm in **(C)**, and 5 μm in **(D)**.

(E) and **(F)** TWD1-YFP signals at the cell periphery colocalize with PM marker FM4-64 (**[E]**; see inset for close-up) and these signals are partially nonoverlapping with ER marker hexyl rhodamine B (**[F]**; see inset for close-up). Note, yellow **(E)** and green PM signals in insets of merged pictures **(F)** indicate PM signals in addition to ER signals for TWD1-YFP. Bar = 10 μm.

(G) Phenotypes of 25 d after germination wild type (Col Wt), *TWD1* loss- (*twd1-3*) and gain-of-function mutants, TWD1-YFP, and YFP-TWD1. DAG, days after germination. Bar = 2 cm.

(H) Functional interaction between TWD1 and ABCB1 Rluc and YFP fusions using transfected tobacco leaves assayed by BRET. Note absence of significant BRET signals with unrelated PM controls, PIRK and PIP2A, and vacuolar control, TT12. Data are means ± SE (n = 4).

Positive BRET ratios for YFP and Rluc combinations of ABCB1 and TWD1 expressed transiently in tobacco (Figure 6; Henrichs et al., 2012) and stably in *Arabidopsis* (see Supplemental Figure 11 online), respectively, indicate functional interaction in planta. This verifies previous findings demonstrating TWD1–ABCB1 interaction by means of coimmunoprecipitation and NPA affinity chromatography (Geisler et al., 2003). However, while biochemical methods always harbor the risk of nonrelevant complex formation during solubilization, this is excluded using BRET. Moreover, BRET offers the option to demonstrate specificity by employing internal controls: TWD1–ABCB1 interactions are specific as YFP or Rluc fusions of unrelated PM controls, PIRK (Henrichs et al., 2012) and PIP2A (Nelson et al., 2007), or tonoplast and nuclear controls, TT12 (Marinova et al., 2007) and STH (Subramanian et al., 2006), did not result in significant BRET ratios in *Arabidopsis* and tobacco (Figure 6H; see Supplemental Figure 11 online). However, in agreement with coimmunolocalization analyses (Figure 4) showing weak colocalization in the stele, PIN1 did weakly but significantly interact with TWD1 (see Supplemental Figure 11 online). This aspect is currently under investigation.

In line with the fact that colocalizations were found only in distinct cells or cell files where they were limited to discrete domains, BRET ratios were a factor 10 lower compared with the yeast system (Bailly et al., 2008) but are in the range typically found for mammalian complexes. Moreover, the concept that the TWD1/ABCB1 interaction might be of transient nature (Bailly et al., 2008), which is also supported by the TWD1/ABCB expression stoichiometry (see Supplemental Figure 4 online), could account for lower BRET ratios in planta compared with the unicellular yeast system.

In summary, these data support significant TWD1-ABCB colocalizations and interactions on distinct PM domains that have the potential to account for altered ABCB1-driven auxin transport capacities.

ABCBs Are Delocalized and Degraded in *twd1*

Recent reports suggested ER retention for B1, B19, and ABCB4 (B4), a related facultative IAA in/exporter (Santelia et al., 2005; Terasaka et al., 2005; Geisler and Murphy, 2006; Cho et al., 2007; Yang and Murphy, 2009), in *twd1* as an exclusive basis of the twisted dwarf phenotype (Titapiwatanakun et al., 2009; Wu et al., 2010). In light of the TWD1–ABCB1 interaction on the PM, we reanalyzed B1, B19, and B4 expression in *twd1* using the same lines as Wu et al. (2010) but employed double labeling using other PM and ER markers.

Our results confirm an ER location for all three ABCBs in *twd1-3* but clearly demonstrate that a significant portion of B1, B19, and B4 is still retained at the PM (Figure 7). Moreover, identical laser and microscope settings between the wild type and *twd1-3* imaging revealed that expression of all three ABCBs was strongly downregulated (Figure 7B). The reduction of ABCB expression was similar for B1 and B19, while most B4 was retained in the root cap (Figure 7B) showing clear PM signals. The weakly retained B4 signal in other parts of roots was mostly found on the ER as judged from colocalization with the ER marker hexyl rhodamine B (Figure 7A; see Supplemental Figure 12 online). Furthermore, immunoblot analyses comparing GFP-tagged B1, B4, and B19 in the

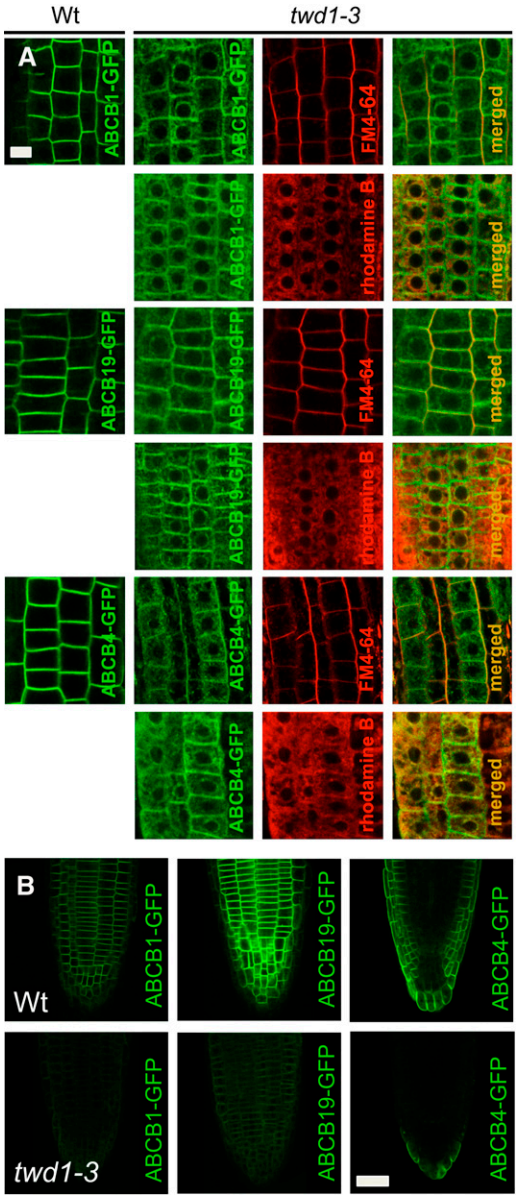

Figure 7. ABCBs Are Delocalized from the PM and Degraded in *twd1*.

(A) B1-, B19-, and B4-GFP are broadly localized to the ER in *twd1-3*, but colocalization with PM and ER markers, FM4-64 (2.5 μM, 10 min staining) and hexyl rhodamine B (rhodamine B; 2 μM, 20 min staining), suggests that a portion resides at the PM. Wt, the wild type. Bar = 10 μm.
(B) Expression of B1-, B19-, and B4-GFP is significantly downregulated in *twd1-3* as revealed by confocal analysis using identical microscope settings. Bar = 50 μm.

wild type and *twd1-3* confirmed a reduced PM presence but also revealed a strong degree of protein degradation (see Supplemental Figure 13 online).

In summary, these data sets suggest that TWD1 affects the presence and degradation of B1, B4, and B19 at the PM employing an unknown mechanism. However, a portion of all three transporters is retained at the PM in the absence of TWD1.

DISCUSSION

TWD1 Resides at ER and PMs and Functionally Interacts with ABCBs at the PM

Two potential modes of action have recently been suggested to be responsible for loss of ABCB functionality in *twd1*: First, TWD1 is essential for the catalytic activation of ABCB-mediated transport by a so far poorly understood mechanism that might involve ABCB phosphorylation (Henrichs et al., 2012) during an interaction taking place at the PM (Bailly et al., 2008). Second, an ER-based, cytoplasmic-oriented TWD1 is responsible for chaperoning ABCB from the ER to the PM (Wu et al., 2010).

Here, using fluorescent protein fusion and immunolocalization, we confirm intracellular ER locations for TWD1 (Figures 5 and 6; see Supplemental Figure 6 online; Wu et al., 2010) but provide three lines of evidence supporting that TWD1 resides as well on the PM (Kamphausen et al., 2002; Geisler et al., 2003): First, PM localizations were verified by coimaging of TWD1:TWD1-CFP with PM markers, FM4-64 and 29-1-GFP, in the first true leaves (see Supplemental Figure 6 online). PM localizations for TWD1:TWD1-CFP and 35S:TWD1-YFP/35S:YFP-TWD1 were further supported by immunoblot analysis of microsomal fractions showing clear overlap with PM markers, PIP and AHA2 (see Supplemental Figure 7 online). We also discovered immunologically lateral PM domains in the epidermis where TWD1 colocalizes widely with the lateral marker PEN3/ABCG36 (Langowski et al., 2010; Ruzicka et al., 2010) and partially with nonpolar PM proteins, BRI1-GFP and ABCB1-GFP (Figure 4). Additionally, we found occasional basal TWD1 labeling in distinct cell files of the root stele that is shared with those of B19-GFP (Figure 4).

These data support a dual localization in the ER and the PM for TWD1 that is regulated in a tissue/cell-specific manner. This is further supported by the finding that expression of TWD1 under the control of the cauliflower mosaic virus 35S promoter results in mixed ER and PM locations in the same cell and ER or PM locations in neighboring cells (Figure 6). Therefore, subcellular differences between 35S:TWD1-YFP and TWD1:TWD1-CFP seem to be caused at least partially by constitutive overexpression. On the contrary, lack of signals during ER protein immunolocalizations is a well-known artifact of fixation.

Second, a PM location is indirectly supported by the fact that BFA treatment leads to colocalization of TWD1 with B1-GFP (Figure 5), B19-GFP/CFP (Figure 5; see Supplemental Figure 10 online), and PEN3-GFP (Figure 5) but not with an ER marker in BFA compartments (Figure 5), reminiscent of PM proteins. In a previous study (Wu et al., 2010) using higher BFA concentrations and a longer incubation time (50 μM BFA for 1.5 h) but the same line, TWD1-CFP was shown to be excluded from BFA bodies. It should be mentioned that our results have been obtained by two independent techniques (fluorescent protein fusion and immunolocalization). However, it is worth mentioning that the above-cited study focused on meristematic root zones that show less BFA compartments in comparison to the elongation zone we were studying (Figures 5A to 5F).

Third, TWD1–ABCB1 interaction was verified subsequently by in planta BRET analysis (Figure 6; see Supplemental Figure 11 online), supporting additionally a PM presence of TWD1, since

ABCB1 has not been reported to reside on the ER in the wild type and shows no ER presence in 35S:ABCB1-YFP *Arabidopsis* plants (Henrichs et al., 2012).

TWD1 Might Have a Dual Function at the PM and the ER

Colocalization and interaction studies support a functional TWD1–ABCB1 interaction that takes place at the PM. However, we believe that the two suggested mechanisms of ABCB regulation, either by PM activation or ER-to-PM secretion, do not necessarily have to be mutually exclusive. Although it is still unclear how a cytoplasmically oriented but ER-anchored TWD1 would be able to perform such a suggested chaperone function during ER-to-PM secretion (Wu et al., 2010) that is commonly associated with the ER lumen (Saijo, 2010), B1, B19, and B4 are indeed widely ER localized in the absence of *TWD1* (Wu et al., 2010; Figure 7; see Supplemental Figure 12 online). However, besides the localization of B1, B19, and B4 at the ER, all three ABCBs are strongly downregulated/degraded in *twd1* (Figure 7; see Supplemental Figure 13 online), implying the plausible concept that ABCBs that are not activated or stabilized by TWD1 at the PM are removed and degraded, most probably at the ER. A coexistence of both mechanisms is further underlined by the fact that the human TWD1 ortholog, FKBP38, also resides functionally at multiple membrane domains, including the ER and mitochondria, where it directs a plethora of functions (Shirane and Nakayama, 2003; Edlich and Lucke, 2011). Like TWD1, FKBP38 has a pair of interacting partners, the anti-apoptotic factors Bcl-2 and Bcl-x(L) (Shirane and Nakayama, 2003). TWD1 was shown to interact with B1 and B19 (Geisler et al., 2003; Bouchard et al., 2006; Bailly et al., 2008) and ABCC1 and ABCC2 (Geisler et al., 2004). This suggested role for FKBP38 in membrane scaffolding and partner activation seems to hold true for TWD1 as well.

Dual ER/PM locations and functionalities of key components of auxin transport or signaling seem to be evolutionarily conserved. The auxin binding protein ABP1 also seems to perform a dual function both in the ER and at the apoplastic side of the PM (Friml and Jones, 2010).

TWD1 Promotes Shootward ABCB-Mediated PAT in the Root

In summary, our data support a model in which TWD1 promotes ABCB1-mediated auxin transport at a functional PM domain that is crucial for auxin-mediated plant growth. In this model, TWD1 would boost lateral, mainly outward-facing, ABCB1-catalyzed auxin export out of the epidermis into the root apoplast (see Supplemental Figure 14 online). First insights into the mechanism of activation of ABCB activity by TWD1 were provided by the finding that TWD1 interacts with AGC kinase PINOID that alters ABCB1 activity by protein phosphorylation (Henrichs et al., 2012).

This functionality of TWD1 might be of special interest for two reasons: First, it would provide a mechanism to minimize apoplastic reflux in tissues with high auxin contents and thus help in separating opposite shoot- and rootward auxin streams between the root epidermis and adjacent cortex on one hand and the stele on the other. This role is supported by the coexpression of TWD1 and ABCB1 in root tissues with high auxin levels (Geisler et al., 2005; Matsuda et al., 2011; see Supplemental Figure 4 online) as well as in young or dividing cells in the leaf epidermis known to be dependent on high auxin levels. Second, promotion of lateral auxin efflux into the apoplast is obviously also in agreement with the acid growth theory that predicts auxin-stimulated, lateral proton extrusion as a molecular mechanism of axial cell expansion (Hager, 2003). This functionality is underpinned by reduced shootward PAT fluxes (Figures 2 and 3) in *twd1* roots causing increased root IAA concentrations resulting in reduced root bending capacities (Figure 2) and enhanced twisting (Figure 1) as part of an overall dwarfed growth phenotype. The latter is supported by the finding that IAA application enhances epidermal root twisting (Figure 1). In that context, this work also provides a mechanistic explanation for the twisted dwarf phenotype that is widely resembled by *ABCB1 ABCB19* loss of function. However, it also offers further evidence that twisting organ phenotypes can be caused by a variety of molecular mechanisms and is not restricted to microtubule defects (Weizbauer et al., 2011).

The more severe *twd1* phenotype in comparison to *abcb1 abcb19* argues that additional transporters, such as ABCB4 (Santelia et al., 2005; Terasaka et al., 2005; Geisler and Murphy, 2006; Cho et al., 2007), or even the close homolog ABCB21, might also be regulated by TWD1 activity. This is further supported by the findings that NPA-sensitive B4 is, like B1 and B19, retained at the ER and degraded in *twd1* (Figure 7; Wu et al., 2010) and that NPA reversal of epidermal twisting is incomplete (Figure 1). On the other hand, TWD1–ABCB interaction was shown to be highly specific since close B1/B19 homologs, such as B2, B10, B13, and B14, do obviously not interact with TWD1 (Geisler et al., 2003). Alternatively, functionalities of other proven TWD1 interactors, like HSP90 (Kamphausen et al., 2002) and calmodulin (Kamphausen et al., 2002; Geisler et al., 2003) or vacuolar ABCC1 and C2 (Geisler et al., 2004), might therefore contribute to the twisted syndrome.

METHODS

Plant Material and Phenotypic Analyses

The following *Arabidopsis thaliana* genotypes were used: wild-type plants of ecotypes Ws wild type, Col wild type (Col-0), and Landsberg *erecta* wild type; mutants *b19-1* and *b1-1 b19-1* (Noh et al., 2003); *b19-3* (Lewis et al., 2007); *b1-100* (Lin and Wang, 2005); *b1-100 b19-3* (Wu et al., 2010); *twd1-1* and *twd1-3* (Geisler et al., 2003); and *pin2 b1 b19* (Mravec et al., 2008). Transgenic lines were as follows: B1:B1-GFP and B19:B19-GFP (Mravec et al., 2008), B4:B4-GFP (Cho et al., 2007), 35S:HA-TWD1 (Geisler et al., 2003), PIN1:PIN1-GFP and PIN2:PIN2-GFP (Abas et al., 2006), DR5:GFP (Ottenschläger et al., 2003), PEN3/ABCG36:PEN3/ABCG36-GFP (Stein et al., 2006), BRI1:BRI1-GFP (Geldner et al., 2007), TWD1-CFP, TWD1-CFP/29-1-GFP, TWD1-CFP/ER-YFP, and B4:B4-GFP in *twd1-3* (Wu et al., 2010). Transgenic lines that were crossed into *twd1-3* and homozygous for the transgene in the F3 generation were used. The TWD1-YFP/B19-CFP line was made by transformation of B19:B19-CFP construct into the 35S:TWD1-YFP line; the B19:B19-CFP construct was generated by subcloning the entire B19:B19-GFP sequence (Mravec et al., 2008) into pMOA34 using *Kpn*I-*Not*I, removing the GFP by *Asc*I-*Xma*I and inserting CFP into the same cloning sides.

In analogy to HA-TWD1 (Geisler et al., 2003) for HA-TWD1-Ct constructs, the 9–amino acid–long HA tag was fused genetically to amino acids 1 to 337 of *TWD1* cDNA and inserted into the binary vector pGPTV-KAN. The resulting binary construct was used to transform *Arabidopsis twd1-3* via vacuum infiltration.

Seedlings were grown on vertical plates containing 0.5× Murashige and Skoog media, 1% Suc, and 0.7% phytagar in the dark or at 8 h (short day), 16 h (long day), or 24 h (constant) light per day. Growth parameters were quantified as by Kim et al. (2010). A detailed phenotypic and developmental analysis of *twd1-3*, HA-TWD1, and HA-TWD1-C_t was performed as by Boyes et al. (2001).

Orientation of epidermal layers (angles to the growth direction) was quantified microscopically using agarose imprints. Root gravitropism was analyzed as by Bailly et al. (2008). All experiments were performed at least in triplicate with 30 to 40 seedlings per each experiment.

Localization Analysis and Confocal Microscopy

Whole-mount immunolocalizations in 5 d after germination *Arabidopsis* roots were performed as described (Friml et al., 2003). Specimens were viewed under a TCS SP2 AOBS confocal laser scanning microscope with a 63/1.4 objective. Conditions for imaging were set as 488-nm excitation, collecting bandwidth at 500 to 552 nm for GFP, 405-nm excitation, collecting bandwidth at 410 to 470 nm for 4′,6-diamidino-2-phenylindole (DAPI), 561-nm excitation, and collecting bandwidth at 571 to 630 nm for CY3. Sequential scanning mode was used for imaging GFP and DAPI signal, and CY3 and DAPI was imaged simultaneously. Images were acquired with the Leica confocal software 2.00. Antiserum concentrations were as follows: anti-TWD1 (1:500), anti-PIN1,2 (1:500), and CY3-conjugated anti-rabbit (1:600; Dianova). Anti-TWD1 antibodies were raised against two synthetic peptides covering amino acids 28 to 41 (anti-TWD1$^{1075,\ 1076}$) and 56 to 70 (anti-TWD1$^{1077,\ 1078}$) of the PPIase domain. Peptides and each of two independent polyclonal antisera in rabbits were produced by Operon.

For all other confocal laser scanning microscopy work, Leica TCS SP2 or Leica TCS SP5 equipment was used. Various confocal settings were set to record the emission of GFP (excitation at 488 nm; emission of 498 to 530 nm), CFP (excitation at 458 nm; emission of 468 to 500 nm), YFP (excitation at 514 nm; emission of 524 to 550 nm), and FM4-64 and hexyl rhodamine B (excitation of 543 nm; emission at 580 to 640 nm).

Analysis of IAA Fluxes

A platinum microelectrode was used to monitor IAA fluxes in *Arabidopsis* roots as described previously (Mancuso et al., 2005). DR5:GFP signals in 5 d after germination seedlings in *Arabidopsis* were observed as described (Bailly et al., 2008).

BRET Analyses

TWD1 and ABCB1 cDNAs were amplified by PCR using the following primers: TWD1-UP, 5′-ATGGATGAATCTCTGGAGCATCAA-3′; TWD1-LP, 5′-ATCTGCTTTAACTCTGTGGCGTCG-3′; ABCB1-UP, 5′-ATGGATAATG-ACGGTGGTGCTCCTCC-3′; and ABCB1-LP, 5′-AGCATCATCTTCCTTAA-CCCTAGAAC-3′. PCR fragments were inserted into pCR8-TOPO (Invitrogen) and transferred into compatible BRET destination vectors, pPZP222 and pBIN19 (Subramanian et al., 2006), by Gateway recombination (Invitrogen). For BRET analysis, ABCB1- and TWD1- Rluc/YFP combinations were transformed into *abcb1* and *twd1* mutant lines, and homozygous combinations were crossed with control Rluc/YFP lines. Alternatively, *Nicotiana benthamiana* leaves were *Agrobacterium tumefaciens* coinfiltrated with BRET construct combinations (or corresponding empty vector controls) using standard protocols, and microsomal fractions were prepared 4 d after inoculation. BRET signals were recorded from microsomes (each ~10 μg) in the presence of 5 μM coelenterazine (Biotium), and BRET ratios were calculated as described previously (Bailly et al., 2008). The results are the average of 10 readings collected every minute, presented as average values from a minimum of three independent experiments (independent *Agrobacterium* infiltrations) each with four replicates.

Data Analysis

Data were analyzed using Prism 5.0 (GraphPad Software). Confocal images were processed in Adobe Photoshop CS3 (Adobe Systems) and quantified using ImageJ 1.43 with vertically oriented original TIFF file pixel area or pixel columns mean gray values.

Accession Numbers

Sequence data from this article can be found in the Arabidopsis Genome Initiative or GenBank/EMBL databases under the following accession numbers: TWD1, At3g21640; ABCB1 (formerly PGP1), At2g36910; ABCB19 (formerly MDR1 or PGP19), At3g28860; ABCB4 (formerly MDR4 or PGP4), At2g47000; PIN1, At1g73590; PIN2, At5g57090; ABCG36 (formerly PEN3 or PDR8), At1g59870; and BRI1, At4g39400.

Supplemental Data

The following materials are available in the online version of this article.

Supplemental Figure 1. Quantification of Epidermal DR5:GFP Signals at the Lower Side of Wild-Type (Col Wt), *twd1-3*, HA-TWD1, and HA-TWD1-Ct Roots upon Gravistimulation.

Supplemental Figure 2. Lugol Stain of *Arabidopsis* Root Tips Indicates No Significant Developmental Defects in *TWD1* and *ABCB* Loss- and Gain-of-Function Roots.

Supplemental Figure 3. Illustration of Construction of Heat Map Presentation of IAA Influx Profiles along Wild-Type Roots.

Supplemental Figure 4. Heat Map Presentation of IAA Influx Profiles along Wild-Type (Ws), *twd1*, and *abcb* Roots (All in the Ws Wild-Type Background) Measured Using an IAA-Specific Microelectrode.

Supplemental Figure 5. TWD1 Immunolocalization Controls.

Supplemental Figure 6. TWD1-CFP Largely Colocalizes with PM Markers in the Epidermis of First True Leaves.

Supplemental Figure 7. Separation of TWD1 Microsomes Prepared from *Arabidopsis* Plants Expressing Tagged TWD1 under Native or Constitutive Promoters Using Discontinuous Sucrose Gradient Centrifugation.

Supplemental Figure 8. TWD1-YFP Fusions Functionally Complement *twd1*.

Supplemental Figure 9. TWD1-YFP Partially Colocalizes with PM Marker FM4-64.

Supplemental Figure 10. TWD1-YFP Colocalizes with PM Marker ABCB19-CFP in the Epidermis of Roots.

Supplemental Figure 11. Functional Interaction between TWD1 and ABCB1.

Supplemental Figure 12. ABCB4 Is Widely Delocalized from the PM to the ER in the Meristematic Zone.

Supplemental Figure 13. ABCB1-, ABCB4-, and ABCB19-GFP Are Degraded in *twd1*.

Supplemental Figure 14. Model of the Role of TWD1 in Promoting Lateral ABCB-Mediated Auxin Transport in the Root.

ACKNOWLEDGMENTS

We would thank Vincent Vincenzetti and Laurence Charrier for excellent technical assistance, A. von Arnim for the donation of BRET vectors, E. Spalding for TWD1-CFP, TWD1-CFP/29-1-GFP/ER-YFP, and ABCB4-GFP lines, M. Palmgren for discussion and support, and E. Martinoia for TT12 cDNA, support, and mentorship. Imaging data were partially collected at the Center for Advanced Bioimaging, University of Copenhagen, Denmark. This work was supported by grants from the Novartis Foundation (to M.G.), from the Danish Research School for Biotechnology (to M.G. and A.S.), from the Forschungskredit of the University of Zurich (to A.B.), from the Pool de Recherche of the University of Fribourg (to M.G.), and from the Swiss National Funds (to M.G.). M.G. dedicates this work to his father, who passed away during the resubmission process.

AUTHOR CONTRIBUTIONS

M.G., A.B., and B.W. designed the research. S.H. and B.W. analyzed root twisting. S.H. analyzed statocysts. M.M. provided anti-TWD1. B.W. created B19-CFP and BRET constructs and BRET *Arabidopsis* lines. B.W. and A.S. performed confocal imaging of TWD1-ABCB colocations. E.A. and S.M. recorded IAA electrode data. A.B. analyzed DR5:GFP expression and reanalyzed IAA electrode data. B.W. and A.B. analyzed BRET interactions. M.Z. and J.F. performed TWD1 co-immunolocalizations. M.G., B.W., and A.B. wrote the article.

Received October 5, 2012; revised December 5, 2012; accepted December 20, 2012; published January 15, 2013.

REFERENCES

Abas, L., Benjamins, R., Malenica, N., Paciorek, T., Wiśniewska, J., Moulinier-Anzola, J.C., Sieberer, T., Friml, J., and Luschnig, C. (2006). Intracellular trafficking and proteolysis of the *Arabidopsis* auxin-efflux facilitator PIN2 are involved in root gravitropism. Nat. Cell Biol. **8:** 249–256. Erratum. Nat. Cell Biol. **8:** 424.

Bailly, A., Sovero, V., Vincenzetti, V., Santelia, D., Bartnik, D., Koenig, B.W., Mancuso, S., Martinoia, E., and Geisler, M. (2008). Modulation of P-glycoproteins by auxin transport inhibitors is mediated by interaction with immunophilins. J. Biol. Chem. **283:** 21817–21826.

Blakeslee, J.J., et al. (2007). Interactions among PIN-FORMED and P-glycoprotein auxin transporters in *Arabidopsis*. Plant Cell **19:** 131–147.

Bouchard, R., Bailly, A., Blakeslee, J.J., Oehring, S.C., Vincenzetti, V., Lee, O.R., Paponov, I., Palme, K., Mancuso, S., Murphy, A.S., Schulz, B., and Geisler, M. (2006). Immunophilin-like TWISTED DWARF1 modulates auxin efflux activities of *Arabidopsis* P-glycoproteins. J. Biol. Chem. **281:** 30603–30612.

Boyes, D.C., Zayed, A.M., Ascenzi, R., McCaskill, A.J., Hoffman, N.E., Davis, K.R., and Görlach, J. (2001). Growth stage-based phenotypic analysis of *Arabidopsis*: A model for high throughput functional genomics in plants. Plant Cell **13:** 1499–1510.

Cho, M., Lee, S.H., and Cho, H.T. (2007). P-glycoprotein4 displays auxin efflux transporter-like action in *Arabidopsis* root hair cells and tobacco cells. Plant Cell **19:** 3930–3943.

Christie, J.M., et al. (2011). phot1 inhibition of ABCB19 primes lateral auxin fluxes in the shoot apex required for phototropism. PLoS Biol. **9:** e1001076.

Edlich, F., and Lucke, C. (2011). From cell death to viral replication: The diverse functions of the membrane-associated FKBP38. Curr. Opin. Pharmacol. **11:** 348–353.

Friml, J., Benková, E., Mayer, U., Palme, K., and Muster, G. (2003). Automated whole mount localisation techniques for plant seedlings. Plant J. **34:** 115–24.

Friml, J., and Jones, A.R. (2010). Endoplasmic reticulum: The rising compartment in auxin biology. Plant Physiol. **154:** 458–462.

Galván-Ampudia, C.S., and Offringa, R. (2007). Plant evolution: AGC kinases tell the auxin tale. Trends Plant Sci. **12:** 541–547.

Geisler, M., and Bailly, A. (2007). Tête-à-tête: The function of FKBPs in plant development. Trends Plant Sci. **12:** 465–473.

Geisler, M., et al. (2005). Cellular efflux of auxin catalyzed by the *Arabidopsis* MDR/PGP transporter AtPGP1. Plant J. **44:** 179–194.

Geisler, M., Girin, M., Brandt, S., Vincenzetti, V., Plaza, S., Paris, N., Kobae, Y., Maeshima, M., Billion, K., Kolukisaoglu, U.H., Schulz, B., and Martinoia, E. (2004). *Arabidopsis* immunophilin-like TWD1 functionally interacts with vacuolar ABC transporters. Mol. Biol. Cell **15:** 3393–3405.

Geisler, M., et al. (2003). TWISTED DWARF1, a unique plasma membrane-anchored immunophilin-like protein, interacts with *Arabidopsis* multidrug resistance-like transporters AtPGP1 and AtPGP19. Mol. Biol. Cell **14:** 4238–4249.

Geisler, M., and Murphy, A.S. (2006). The ABC of auxin transport: The role of p-glycoproteins in plant development. FEBS Lett. **580:** 1094–1102.

Geldner, N., Hyman, D.L., Wang, X., Schumacher, K., and Chory, J. (2007). Endosomal signaling of plant steroid receptor kinase BRI1. Genes Dev. **21:** 1598–1602.

Hager, A. (2003). Role of the plasma membrane H+-ATPase in auxin-induced elongation growth: Historical and new aspects. J. Plant Res. **116:** 483–505.

Hashimoto, T. (2002). Molecular genetic analysis of left-right handedness in plants. Philos. Trans. R. Soc. Lond. B Biol. Sci. **357:** 799–808.

Henrichs, S., et al. (2012). Regulation of ABCB1/PGP1-catalysed auxin transport by linker phosphorylation. EMBO J. **31:** 2965–2980.

Kamphausen, T., Fanghänel, J., Neumann, D., Schulz, B., and Rahfeld, J.U. (2002). Characterization of *Arabidopsis thaliana* AtFKBP42 that is membrane-bound and interacts with Hsp90. Plant J. **32:** 263–276.

Kim, J.Y., Henrichs, S., Bailly, A., Vincenzetti, V., Sovero, V., Mancuso, S., Pollmann, S., Kim, D., Geisler, M., and Nam, H.G. (2010). Identification of an ABCB/P-glycoprotein-specific inhibitor of auxin transport by chemical genomics. J. Biol. Chem. **285:** 23309–23317.

Langowski, L., Růzicka, K., Naramoto, S., Kleine-Vehn, J., and Friml, J. (2010). Trafficking to the outer polar domain defines the root-soil interface. Curr. Biol. **20:** 904–908.

Lewis, D.R., Miller, N.D., Splitt, B.L., Wu, G., and Spalding, E.P. (2007). Separating the roles of acropetal and basipetal auxin transport on gravitropism with mutations in two *Arabidopsis* multidrug resistance-like ABC transporter genes. Plant Cell **19:** 1838–1850.

Lin, R., and Wang, H. (2005). Two homologous ATP-binding cassette transporter proteins, AtMDR1 and AtPGP1, regulate *Arabidopsis* photomorphogenesis and root development by mediating polar auxin transport. Plant Physiol. **138:** 949–964.

Mancuso, S., Marras, A.M., Magnus, V., and Baluska, F. (2005). Noninvasive and continuous recordings of auxin fluxes in intact root apex with a carbon nanotube-modified and self-referencing microelectrode. Anal. Biochem. **341:** 344–351.

Marinova, K., Pourcel, L., Weder, B., Schwarz, M., Barron, D., Routaboul, J.M., Debeaujon, I., and Klein, M. (2007). The *Arabidopsis* MATE transporter TT12 acts as a vacuolar flavonoid/H+-antiporter active in proanthocyanidin-accumulating cells of the seed coat. Plant Cell **19:** 2023–2038.

Matsuda, S., Kajizuka, T., Kadota, A., Nishimura, T., and Koshiba, T. (2011). NPH3- and PGP-like genes are exclusively expressed in

the apical tip region essential for blue-light perception and lateral auxin transport in maize coleoptiles. J. Exp. Bot. **62:** 3459–3466.

Mravec, J., Kubes, M., Bielach, A., Gaykova, V., Petrásek, J., Skůpa, P., Chand, S., Benková, E., Zazímalová, E., and Friml, J. (2008). Interaction of PIN and PGP transport mechanisms in auxin distribution-dependent development. Development **135:** 3345–3354.

Murphy, A.S., Hoogner, K.R., Peer, W.A., and Taiz, L. (2002). Identification, purification, and molecular cloning of N-1-naphthylphthalmic acid-binding plasma membrane-associated aminopeptidases from *Arabidopsis*. Plant Physiol. **128:** 935–950.

Nelson, B.K., Cai, X., and Nebenführ, A. (2007). A multicolored set of in vivo organelle markers for co-localization studies in *Arabidopsis* and other plants. Plant J. **51:** 1126–1136.

Noh, B., Bandyopadhyay, A., Peer, W.A., Spalding, E.P., and Murphy, A.S. (2003). Enhanced gravi- and phototropism in plant mdr mutants mislocalizing the auxin efflux protein PIN1. Nature **423:** 999–1002.

Ottenschläger, I., Wolff, P., Wolverton, C., Bhalerao, R.P., Sandberg, G., Ishikawa, H., Evans, M., and Palme, K. (2003). Gravity-regulated differential auxin transport from columella to lateral root cap cells. Proc. Natl. Acad. Sci. USA **100:** 2987–2991.

Petersson, S.V., Johansson, A.I., Kowalczyk, M., Makoveychuk, A., Wang, J.Y., Moritz, T., Grebe, M., Benfey, P.N., Sandberg, G., and Ljung, K. (2009). An auxin gradient and maximum in the *Arabidopsis* root apex shown by high-resolution cell-specific analysis of IAA distribution and synthesis. Plant Cell **21:** 1659–1668.

Robert, H.S., and Friml, J. (2009). Auxin and other signals on the move in plants. Nat. Chem. Biol. **5:** 325–332.

Ruzicka, K., et al. (2010). *Arabidopsis PIS1* encodes the ABCG37 transporter of auxinic compounds including the auxin precursor indole-3-butyric acid. Proc. Natl. Acad. Sci. USA **107:** 10749–10753.

Saijo, Y. (2010). ER quality control of immune receptors and regulators in plants. Cell. Microbiol. **12:** 716–724.

Santelia, D., Vincenzetti, V., Azzarello, E., Bovet, L., Fukao, Y., Düchtig, P., Mancuso, S., Martinoia, E., and Geisler, M. (2005). MDR-like ABC transporter AtPGP4 is involved in auxin-mediated lateral root and root hair development. FEBS Lett. **579:** 5399–5406.

Shirane, M., and Nakayama, K.I. (2003). Inherent calcineurin inhibitor FKBP38 targets Bcl-2 to mitochondria and inhibits apoptosis. Nat. Cell Biol. **5:** 28–37.

Stein, M., Dittgen, J., Sánchez-Rodríguez, C., Hou, B.H., Molina, A., Schulze-Lefert, P., Lipka, V., and Somerville, S. (2006). *Arabidopsis* PEN3/PDR8, an ATP binding cassette transporter, contributes to nonhost resistance to inappropriate pathogens that enter by direct penetration. Plant Cell **18:** 731–746.

Subramanian, C., Woo, J., Cai, X., Xu, X., Servick, S., Johnson, C.H., Nebenführ, A., and von Arnim, A.G. (2006). A suite of tools and application notes for in vivo protein interaction assays using bioluminescence resonance energy transfer (BRET). Plant J. **48:** 138–152.

Swarup, R., Kramer, E.M., Perry, P., Knox, K., Leyser, H.M., Haseloff, J., Beemster, G.T., Bhalerao, R., and Bennett, M.J. (2005). Root gravitropism requires lateral root cap and epidermal cells for transport and response to a mobile auxin signal. Nat. Cell Biol. **7:** 1057–1065.

Terasaka, K., Blakeslee, J.J., Titapiwatanakun, B., Peer, W.A., Bandyopadhyay, A., Makam, S.N., Lee, O.R., Richards, E.L., Murphy, A.S., Sato, F., and Yazaki, K. (2005). PGP4, an ATP binding cassette P-glycoprotein, catalyzes auxin transport in *Arabidopsis thaliana* roots. Plant Cell **17:** 2922–2939.

Titapiwatanakun, B., et al. (2009). ABCB19/PGP19 stabilises PIN1 in membrane microdomains in *Arabidopsis*. Plant J. **57:** 27–44.

Vanneste, S., and Friml, J. (2009). Auxin: A trigger for change in plant development. Cell **136:** 1005–1016.

Weizbauer, R., Peters, W.S., and Schulz, B. (2011). Geometric constraints and the anatomical interpretation of twisted plant organ phenotypes. Front. Plant Sci. **2:** 62.

Wisniewska, J., Xu, J., Seifertová, D., Brewer, P.B., Ruzicka, K., Blilou, I., Rouquié, D., Benková, E., Scheres, B., and Friml, J. (2006). Polar PIN localization directs auxin flow in plants. Science **312:** 883.

Wu, G., Otegui, M.S., and Spalding, E.P. (2010). The ER-localized TWD1 immunophilin is necessary for localization of multidrug resistance-like proteins required for polar auxin transport in *Arabidopsis* roots. Plant Cell **22:** 3295–3304.

Yang, H., and Murphy, A.S. (2009). Functional expression and characterization of *Arabidopsis* ABCB, AUX 1 and PIN auxin transporters in *Schizosaccharomyces pombe*. Plant J. **59:** 179–191.